Eur. Phys. J. Plus (2023) 138:49
https://doi.org/10.1140/epjp/s13360-023-03678-y

THE EUROPEAN PHYSICAL JOURNAL PLUS

Regular Article

Theoretical investigation of nonlinear optical properties of Mathieu quantum well

E. B. Al[1,a], **A. J. Peter**[2,b], **M. E. Mora-Ramos**[3,c], **F. Ungan**[1,d]

[1] Department of Physics, Faculty of Science, Sivas Cumhuriyet University, 58140 Sivas, Turkey
[2] P.G and Research Department of Physics, Government Arts College, Melur, Madurai 625 106, India
[3] Centro de Investigación en Ciencias-IICBA, Universidad Autónoma del Estado de Morelos, Ave. Universidad 1001, 62209 Cuernavaca, Morelos, Mexico

Received: 22 September 2022 / Accepted: 9 January 2023

Abstract In this study, for the first time, the effect of externally applied static electric, magnetic, and non-resonant THz intense laser fields on nonlinear optical properties such as the total optical absorption coefficients (TOACs) and relative refractive index changes (RRICs) in a GaAs/AlGaAs Mathieu quantum well are theoretically investigated in detail. Moreover, the influence of the adjustable physical parameters, linked to the potential shape of the structure, on the nonlinear optical properties of the system is also investigated. For this, firstly, the electronic subband energy levels of the Mathieu quantum well, and their envelope wave functions, are calculated using the diagonalization method within the framework of the effective mass and parabolic single-band approximations. Then, the outcome of the iterative solution of compact-density-matrix formalism is used to obtain the nonlinear optical properties of the structure. The obtained numerical results show that the increase in both the structure parameters and the value of the electric and magnetic field shifted the positions of the TOACs and RRICs peaks towards higher energies (blue-shift). On the other hand, the increase in the value of the intense laser field shifted the peak positions to lower energy levels (red-shift). The determination of the functional range for the optical properties of the Mathieu quantum well, using both the structure parameters and the external fields, is an important gain in terms of providing the initial parameters for experimental studies.

1 Introduction

Nowadays, low-dimensional semiconductor quantum systems such as quantum wells (QWs), wires, and dots have attracted the attention of many scientific communities due to their unique electronic and optical properties [1–10]. For instance, QWs were largely employed in the fabrication of quantum devices such as the field-effect transistor (FET), resonant tunneling diodes (RTD), quantum cascade lasers, as well as a large variety of new generations of optoelectronic devices [11–16]. The electronic energy levels in QW systems are very sensitive to structure geometry and other physical parameters (hydrostatic pressure, temperature, quantum size, etc.), including applied external fields. In addition, the doping process is still a very promising technique that is largely used by researchers to modify the subband energy levels and consequently the optical properties of various QW systems [17–25].

The investigation of QW structures is relevant given their possible applications in technological devices. As mentioned, the shape of the QW profile affects the physical properties of the systems. Besides, understanding the linear and nonlinear optical properties of the QW systems is critical because the optical properties of the structure are strongly affected by the structure parameters and the applied external fields. For this reason, theoretical and experimental research has been carried out to obtain the linear and nonlinear properties of this structure at different structure parameters and the applied external fields [26–32]. Some of the main studies are as follows: the effect of the electric field on the nonlinear optical properties of QWs [33], the optical absorption in symmetric double parabolic QWs [34], TOACs with Rosen–Morse confinement potential [35], the effect of impurities and optical intensities on the linear and nonlinear optical absorption coefficients (OACs), the RRICs in low-dimensional systems [36], and the OACs and the RICs of the superlattice [37]. The optical properties in double and triple-delta doped GaAs QW were analysed by Dakhlaoui et al. [38]. They showed the impact of external fields on the optical properties of symmetric and asymmetric doping concentrations, especially in controlling the blue- and red-shifts of the total optical absorption. Ungan et al. [17] computed the nonlinear optical properties of a triple-delta doped QW (TDDQW). They demonstrated that the central doped layer plays a crucial role in tuning the amplitude and abscissa of the optical absorption coefficients. In their works, the asymmetricity of the three doped layers constituted an important key to obtaining the red- and blue-shifts.

[a] e-mail: emrebahadiral@hotmail.com (corresponding author)
[b] e-mail: a.john.peter@gmail.com
[c] e-mail: memora@uaem.mx
[d] e-mail: fungan@cumhuriyet.edu.tr

Published online: 20 January 2023

Despite the diversity of the results obtained in the works mentioned throughout this introduction, a rigorous study of optical properties in a Mathieu QW is still lacking. For this reason, in the present paper, we aim to discuss the optical properties such as the TOACs and RRICs produced by the Mathieu QW system under the impact of external fields. Our paper is organized as follows: theoretical background constitutes in Sect. 2. The discussions and comments on the obtained results are summarized in Sect. 3. And finally, the important conclusions are presented in Sect. 4.

2 Theory

We consider an electron confined in a Mathieu QW, which is exposed to static electric and magnetic fields in the presence of a high-frequency, monochromatic intense laser field (ILF) with polarization parallel to the growth direction-$\widehat{z}$ of the structure. Also, we assume that the static electric field is applied parallel to the growth direction of the structure ($\overrightarrow{F} = F\widehat{z}$), while the static magnetic field is applied perpendicular to this electric field ($\overrightarrow{B} = B\widehat{x}$). For this particular configuration, the vector potential is $\overrightarrow{A}\left(\overrightarrow{r}\right) = -Bz\widehat{y}$ in the Landau gauge. Within the framework of the effective mass and parabolic band approximations, the Hamiltonian of an electron confined in a Mathieu QW structure under the effects of these externally applied fields can be expressed as [39].

$$H = \frac{1}{2m_e^*}\left[\vec{p}_e + \frac{e}{c}\vec{A}\right]^2 + \langle V_M(z,\alpha_0)\rangle + e\vec{F}\cdot\vec{z} \tag{1}$$

where m_e^* is the effective mass of the electron in the GaAs material, $\overrightarrow{p}_e$ is the momentum operator of the electron, e is the absolute value of the elementary charge of the electron, c is the speed of light in free space and $V_M(z,\alpha_0)$ is the laser dressed confinement potential given by the following expression [40]

$$\langle V_M(z,\alpha_0)\rangle = \frac{\Omega}{2\pi}\int_0^{2\pi/\Omega} V_M(z+\alpha_0\sin\Omega t)dt \tag{2}$$

where, $\alpha_0 = \frac{eA_0}{m_e^*\Omega}$ is the laser dressing density parameter, A_0 is the optical laser field strength, Ω is the non-resonant frequency of the laser field, and $V_M(z)$ is the Mathieu confinement potential in the absence of high-frequency ILF and it is given by [41]

$$V_M(z) = V_0\left[\sin^2(\eta z) - \cos(\eta z)\right] \tag{3}$$

where, V_0 represents the potential depth and η is the potential width parameter.

The electron wave function corresponding to the Hamiltonian in Eq. (1) can be written as

$$\psi(r) = e^{\vec{k}_\perp\cdot\vec{\rho}}\varphi(z) \tag{4}$$

where $k_\perp = \left(k_x, k_y\right)$ and $\varphi(z)$ satisfies the following one-dimensional Schrödinger equation:

$$\left[\frac{-\hbar^2}{2m_e^*}\frac{d^2}{dz^2} + \frac{e^2B^2}{2m_e^*c^2}\left(z + \frac{c\hbar k_x}{eB}\right)^2 + \langle V_M(z,\alpha_0)\rangle + e\vec{F}\cdot\vec{z}\right]\varphi(z) = \left[E_z - \frac{\hbar^2k_y^2}{2m_e^*}\right]\varphi(z) \tag{5}$$

Under the constraint $k_\perp = 0$, Eq. (5) becomes:

$$\left[\frac{-\hbar^2}{2m_e^*}\frac{d^2}{dz^2} + \frac{e^2B^2Z^2}{2m_e^*c^2} + \langle V_M(z,\alpha_0)\rangle + e\vec{F}\cdot\vec{z}\right]\varphi(z) = E_z\varphi(z) \tag{6}$$

where E_z and $\varphi(z)$ are the energy eigenvalue and eigenfunction of the structure under applied external perturbations, respectively. Using the diagonalization method proposed by Xia and Fan [42], the lower band energy levels of the system and the envelope wave functions corresponding to these energies are obtained numerically by solving Eq. (6). To solve this equation, the eigenfunction of an infinite potential well of width L_∞ is taken as the basis. These functions are as follows [43]:

$$\varphi_n(z) = \sqrt{\frac{2}{L_\infty}}\cos\left(\frac{n\pi z}{L_\infty} - \delta_n\right) \tag{7}$$

where δ_n is

$$\delta_n = \begin{cases} 0, n \text{ is odd} \\ \frac{\pi}{2}, n \text{ is even} \end{cases} \tag{8}$$

so that the wave functions describing the structure under consideration consist of a complete set:

$$\varphi(z) = \sum_{n=1}^{n_p} c_n\varphi_n(z) \tag{9}$$

where c_n are the expansion coefficients. However, for a practical application of the method, we must limit the sum to a finite value (n_p). This means that choosing an appropriate base also plays a role in reducing the number of terms included. In this particular calculation, we used the convergent values of $n_p = 200$ and $L_\infty = 100nm$ for the calculated energy levels, which appear as the eigenvalues of the Hamiltonian matrix.

After obtaining the bound state energies and associated wave functions for the Mathieu QW, we use the outcome of compact density matrix approximation, obtained by the iterative procedure [44–46] to calculate the changes of RRICs and OACs corresponding to transitions between the two subband energy states in the system. For that purpose, we assume that a polarized monochromatic electromagnetic field interacts with a QW. The electric field vector of this optical wave is [47]

$$\vec{E}(t) = 2\vec{E}_0 \cos(\omega t) = \vec{E}_0\left(e^{-i\omega t} + e^{i\omega t}\right) \tag{10}$$

where, ω is the angular frequency of the incident electromagnetic field.

The variation of the matrix elements of the one-electron density operator-$\widehat{\rho}$ due to the time-dependent interaction is given by the Liouville–von Neumann equation [48]:

$$\frac{\partial \hat{\rho}_{ij}(t)}{\partial t} = \frac{1}{i\hbar}\left[\hat{H}_0 - \vec{M}\cdot\vec{E}(t), \hat{\rho}(t)\right]_{ij} - \Gamma_{ij}\left[\hat{\rho}(t) - \hat{\rho}^{(0)}\right]_{ij} \tag{11}$$

where $\widehat{H}_0$ is the Hamiltonian of the system in the absence of electromagnetic field-$E(t)$, $\overrightarrow{M}$ is the electric dipole moment operator and $\Gamma_{ij} = 1/T_{ij}$ (T_{ij} is the intersubband relaxation time) represents the relaxation ratio, which phenomenologically explains the damping caused by electron–phonon, electron–electron and other collision processes. Also, $\widehat{\rho}^{(0)}$ is the unperturbed density operator. Equation (11) can be solved using the standard iterative method

$$\hat{\rho}(t) = \sum_n \hat{\rho}^{(n)}(t) \tag{12}$$

with

$$\frac{\partial \hat{\rho}_{ij}^{(n+1)}(t)}{\partial t} = \frac{1}{i\hbar}\left\{\left[\hat{H}_0, \hat{\rho}^{(n+1)}(t)\right]_{ij} - i\hbar\Gamma_{ij}\hat{\rho}_{ij}^{(n+1)}(t)\right\} - \frac{1}{i\hbar}\left[\vec{M}, \hat{\rho}^{(n)}(t)\right]_{ij}\cdot\vec{E}(t) \tag{13}$$

Furthermore, the electronic polarization of the system due to the electric field can be written up to the third order of E as

$$P(t) = E_0\left(\chi_\omega^{(1)}Ee^{i\omega t} + \chi_0^{(2)}E^2 + \chi_{2\omega}^{(2)}E^2e^{2i\omega t} + \chi_\omega^{(3)}E^3e^{i\omega t} + \chi_{3\omega}^{(3)}E^3e^{3i\omega t} + \ldots\right) \tag{14}$$

where E_0 is the dielectric constant of the vacuum, $\chi_\omega^{(1)}$, $\chi_0^{(2)}$, $\chi_{2\omega}^{(2)}$, $\chi_\omega^{(3)}$ and $\chi_{3\omega}^{(3)}$ are linear, optical rectification, second harmonic generation, third order and third harmonic generation susceptibilities, respectively.

Linear and nonlinear susceptibilities are determined using the same density matrix formalism, and then the corresponding analytical expressions are given as [49]

$$\chi_\omega^{(1)}(\omega) = \frac{\sigma_s\left|M_{ij}\right|^2}{\varepsilon_0\left(E_{ij} - \hbar\omega - i\hbar\Gamma_{ij}\right)} \tag{15}$$

and

$$\chi_\omega^{(3)}(\omega) = \frac{\sigma_s\hbar\omega\left|M_{ij}\right|^2E^2}{\varepsilon_0\left(E_{ij} - \hbar\omega - i\hbar\Gamma_{ij}\right)}\left[\frac{4\left|M_{ij}\right|^2}{\left(E_{ij} - \hbar\omega\right)^2 + \left(\hbar\Gamma_{ij}\right)^2} - \frac{\left|M_{jj} - M_{ii}\right|^2}{\left(E_{ij} - i\hbar\Gamma_{ij}\right)\left(E_{ij} - \hbar\omega - i\hbar\Gamma_{ij}\right)}\right] \tag{16}$$

where, σ_s is the electron density in the QW, $E_{ij} = E_i - E_j$ is the energy difference between the initial and final energy states, $\left|M_{ij}\right| = \left|\langle\varphi_i|ez|\varphi_j\rangle\right|$ represents the absolute value of the off-diagonal matrix elements of the electric dipole moment operator for the z polarization of light and φ_i (φ_j) is the eigenfunction of initial (final) state.

Linear and third-order nonlinear RRICs for intersubband transitions can be calculated from

$$\frac{\Delta n(\omega)}{n_r} = \Re\left[\frac{\chi(\omega)}{2n_r^2}\right] \tag{17}$$

where n_r is the relative refractive index of the structure. Considering Eqs. (15–17), linear and third-order nonlinear RRICs are provided with

$$\frac{\Delta n^{(1)}(\omega)}{n_r} = \frac{\sigma_s\left|M_{ij}\right|^2}{2n_r^2\varepsilon_0}\frac{E_{ij} - \hbar\omega}{\left(E_{ij} - \hbar\omega\right)^2 + \left(\hbar\Gamma_{ij}\right)^2} \tag{18}$$

and

$$\frac{\Delta n^{(3)}(\omega, I)}{n_r} = \frac{-\mu c I \sigma_s |M_{ij}|^4}{n_r^3 \varepsilon_0} \frac{E_{ij} - \hbar\omega}{\left[\left(E_{ij} - \hbar\omega\right)^2 + \left(\hbar\Gamma_{ij}\right)^2\right]^2} \left[1 - \frac{|M_{jj} - M_{ii}|^2 \left[E_{ij}^2 - E_{ij}\left(\hbar\omega + \frac{(\hbar\Gamma_{ij})^2}{E_{ij} - \hbar\omega}\right) - 2\left(\hbar\Gamma_{ij}\right)^2\right]}{4|M_{ij}|^2 \left[E_{ij}^2 + \left(\hbar\Gamma_{ij}\right)^2\right]}\right] \tag{19}$$

where, μ is the permeability of the structure, $I = 2\varepsilon_0 n_r c E^2$ is the optical intensity of the incident electromagnetic wave.

TRRICs are calculated taking into account linear and nonlinear contributions:

$$\frac{\Delta n(\omega, I)}{n_r} = \frac{\Delta n^{(1)}(\omega)}{n_r} + \frac{\Delta n^{(3)}(\omega, I)}{n_r} \tag{20}$$

However, the OACs are expressed by

$$\alpha(\omega) = \omega \sqrt{\frac{\mu}{\varepsilon_r}} I[\varepsilon_0 \chi(\omega)] \tag{21}$$

where, ε_r is the real part of the dielectric permittivity. Linear and third-order nonlinear OACs are provided by

$$\alpha^{(1)}(\omega) = \sqrt{\frac{\mu}{\varepsilon_r}} \frac{\sigma_s |M_{ij}|^2 \hbar\omega\Gamma_{ij}}{\left(E_{ij} - \hbar\omega\right)^2 + \left(\hbar\Gamma_{ij}\right)^2} \tag{22}$$

and

$$\alpha^{(3)}(\omega, I) = -\sqrt{\frac{\mu}{\varepsilon_r}} \frac{2I}{n_r \varepsilon_0 c} \frac{\sigma_s |M_{ij}|^4 \hbar\omega\Gamma_{ij}}{\left[\left(E_{ij} - \hbar\omega\right)^2 + \left(\hbar\Gamma_{ij}\right)^2\right]^2} \left[1 - \frac{|M_{jj} - M_{ii}|^2}{4|M_{ij}|^2} \frac{3E_{ij}^2 - 4E_{ij}\hbar\omega + \hbar^2\left(\omega^2 - \Gamma_{ij}^2\right)}{E_{ij}^2 + \left(\hbar\Gamma_{ij}\right)^2}\right] \tag{23}$$

TOACs is calculated considering linear and nonlinear contributions:

$$\alpha(\omega, I) = \alpha^{(1)}(\omega) + \alpha^{(3)}(\omega, I) \tag{24}$$

3 Result and discussion

The physical values of simulation input parameters are listed as: $m_e^* = 0.067 m_0$ (m_0 is the free electron mass), $c = 3 \times 10^8$m/s, $e = 1.602 \times 10^{-19}$ C, $\hbar = 1.056 \times 10^{-34}$ Js, $\sigma_v = 1 \times 10^{23}\text{m}^{-3}$, $\mu = 4\pi \times 10^7 \text{Hm}^{-1}$,$\varepsilon = 12.58$, $\varepsilon_0 = 8.854 \times 10^{-12}$, $I = 0.1 \frac{\text{MW}}{\text{cm}^2}$, $\tau_{12} = 0.2ps$, $n_r = 3.2$, and the effective QW width is 20 nm. The influence of external perturbations such as ILF, static electric and magnetic fields as well as structure parameters on the TOACs and RRICs of the Mathieu QW system is investigated in this section.

Figure 1 shows the first two subband energy levels, the square of the wavefunctions corresponding to these energy levels, and the confining potential profile of the Mathieu QW in the absence of external perturbations. In Fig. 1a, we have presented these electronic properties of the structure with a fixed barrier height as a function of position for two different potential width parameter values. The black line represents the confinement potential, the red line refers to the ground state of the electron level, and the blue line represents the first excited state electron level. In all the figures, the dotted line refers to the potential width parameter of 0.05 nm^{-1}, whereas the solid line represents the potential width parameter of 0.1 nm^{-1}. It is observed that the confinement potential, the energies of ground state electron level, and the first excited state level increase as the potential width parameter increases. Figure 1b presents the variation of confined energies and confinement potential as a function of position for various barrier heights of Mathieu QW with a fixed potential width parameter. As can be seen, a low barrier height when z is small, and a high barrier height when z is large creates a greater confinement potential. This change in confinement potential oppositely affects the excited state energy, while the ground state energy is larger for smaller barrier height for all z values. It is concluded that the subband energy levels and the confinement potential can be modified by the potential width parameter and the barrier height.

Figure 2 shows the variations of subband energy levels and confinement potential of the Mathieu QW with a constant potential width parameter and barrier height in the presence of external perturbations. In this figure, the black line represents the confinement potential, the red line refers to the ground state of the electron level, and the blue line represents the first excited state of the electron level. Figure 2a displays the variation of subband energy levels and confinement potential as a function of position in the presence of an electric field without the application of magnetic field and ILF. It is observed that the confined energies and confinement potential are found to increase with the electric field. The same observation is also noted when the magnetic field is applied in the system, and it is shown in Fig. 2b. When we look at Fig. 2c, the ILF causes an increase in the confinement potential at small z values, while it causes a decrease at large z values. While ILF also causes an increase in ground state energy for all z values, it affects the excited state energy differently at different z values.

In Fig. 3, we present the variation of TOACs with the incident photon energy in the absence of external perturbations. This coefficient results from the superposition of the linear (positive, Eq. (22)) and third-order nonlinear (negative, Eq. (23)) terms. This

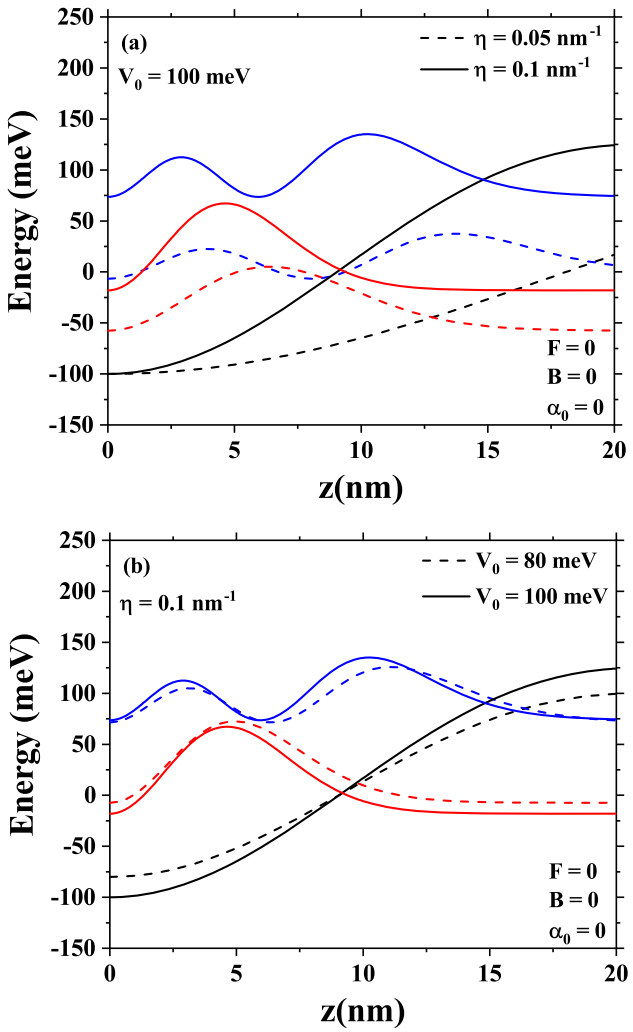

Fig. 1 Variation of subband energy levels and confinement potential as a function of position in the absence of external perturbations; Fig. 1a is for various potential width parameter values of Mathieu QW with a fixed barrier height; Fig. 1b is for various barrier heights of Mathieu QW with a fixed potential width parameter

means an overall reduction in value, compared to the sole linear contribution. Figure 3a brings out the variation of TOACs with the photon energy for various potential width parameter values of Mathieu QW with a fixed barrier height. Here, the electric field, magnetic field, and laser dressing parameters are kept at zero. It is observed that the peak value of the TOACs suffers a blue shift when the structure value is increased. It is because increasing the potential width parameter enhances the energy difference between the ground and the first excited states. It is also seen that the peak amplitude of TOAC increases when the potential width parameter increases. This is entirely due to the fact that the f_{12} increases with increasing potential width parameter. The variation of TOACs with the incident photon energy for various barrier heights of Mathieu QW with a fixed potential width parameter is shown in Fig. 3b. The maximum value of TOACs increase with the increase in barrier height of the well. Moreover, it moves towards higher energies. This trend of peak position shifting to high energy is due to the enhancement of energy difference between the ground state and first excited state with the increase in potential barrier [50]. Table 1 can be checked for detailed review.

Figure 4 shows the variation of TOACs with the incident photon energy in the presence of external fields for a constant potential width parameter and barrier height in Mathieu QW. It is found that the TOACs vary considerably with the inclusion of external perturbations. Figure 4a shows the variation of TOACs as a function of photon energy in the presence of an electric field without a magnetic field and ILF. The increase in electric field forms a blueshift in the resonance peaks, that is, its maximum position shifts towards the higher energies. Further, it is noted that the amplitude of the TOACs diminishes with the enhancement of the electric field. It is because of the increase of repulsion of effective potential and the difference in energies enhances with the increase in an electric field. Figure 4b shows the variation of TOACs as a function of photon energy in the presence of a magnetic field without an electric field and ILF. Increasing the magnetic field both shifts the peak position to blue and causes the peak amplitudes to increase. Because with the increase of the magnetic field, both the difference between the energies and also f_{12} increases. Figure 4c shows the change of TOAC as a function of photon energy for the laser dressing parameter, without a magnetic field and electric field. It is found from the figure that the peak value of TOACs decreases with the increment of the laser dressing parameter. It is concluded

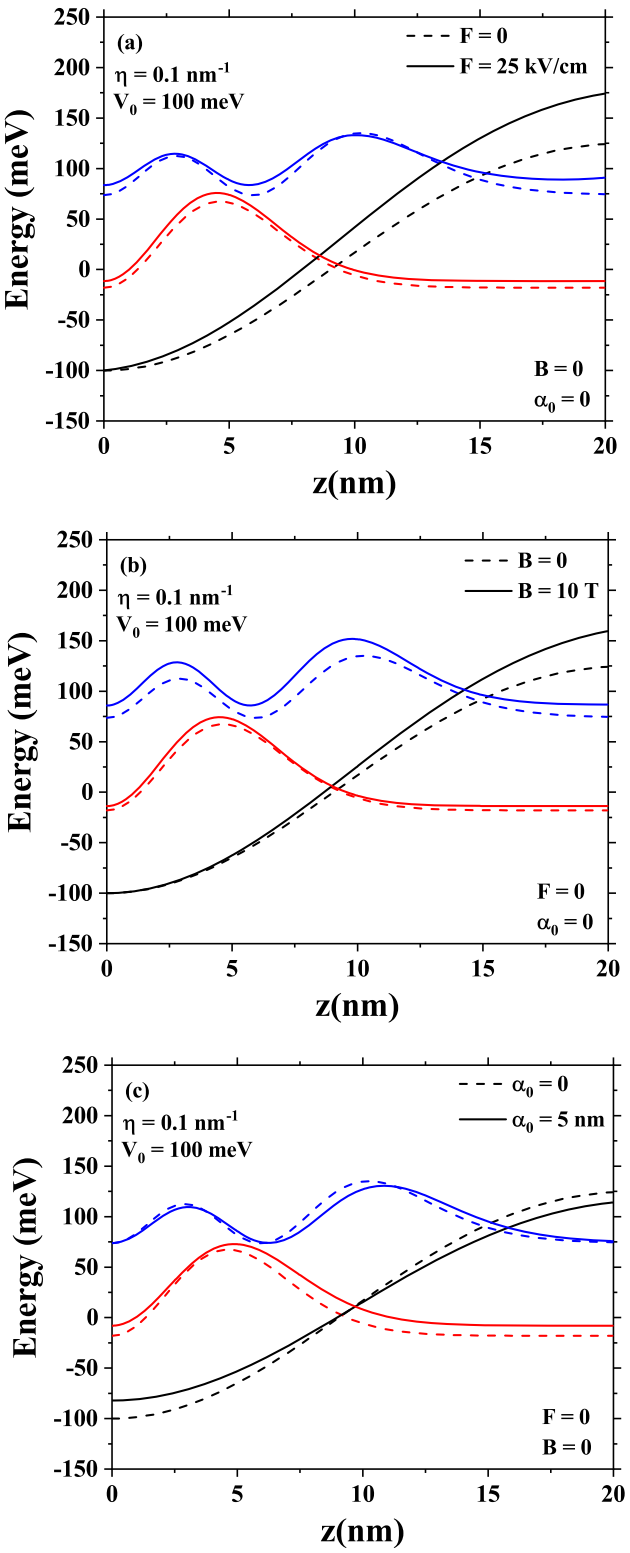

Fig. 2 Variation of subband energy levels and confinement potential with a function of the position for a constant potential width parameter and barrier height of Mathieu QW system; Fig. 2a shows the variation in the presence of electric field without magnetic field and intense laser field; Fig. 2b shows the variations in the presence of magnetic field without electric field and intense laser field; Fig. 2c shows the variation in the presence of intense laser field without magnetic field and electric field

that the peak position shifts towards the lower energies making the redshift. This is owing to the reduction of the energy difference between the initial and the final levels with the increase in the laser dressing parameter.

In Fig. 5, we present the variation of RRICs with the photon energy in the absence of external perturbations. The RRICs are associated with the intersubband transition energy, which is shown here. The RRICs and TOACs occur when the incident photon energies are similar to the intersubband optical transition energies. It happens to owe to the greater values of dipole matrix elements

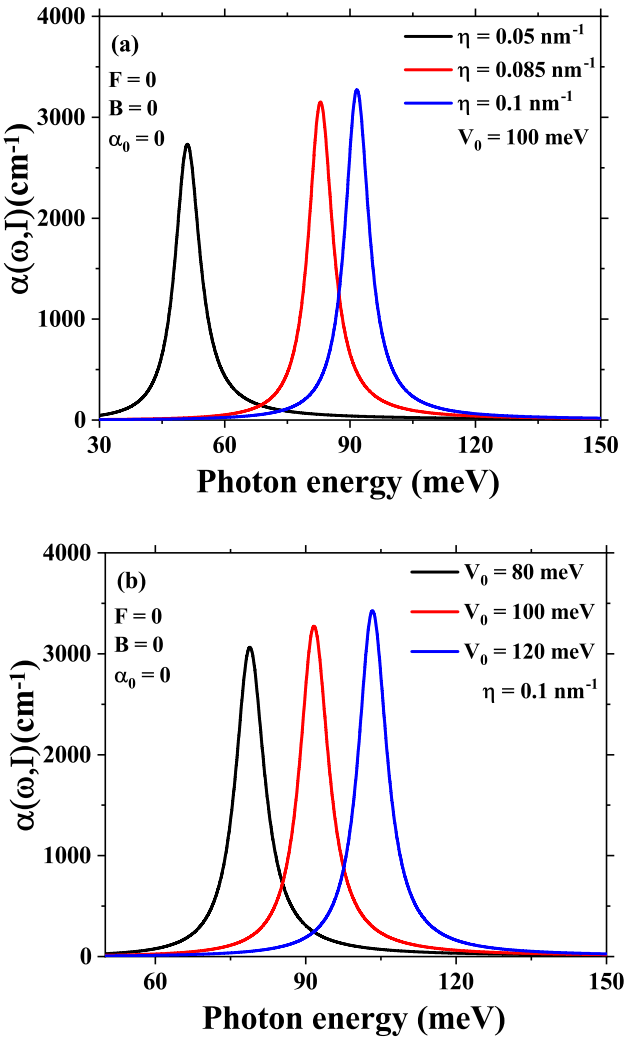

Fig. 3 Variation of TOACs with the photon energy in the absence of external perturbations. Figure 3a is for various potential width parameter values of Mathieu QW with a fixed barrier height. Figure 3b is for various barrier heights of Mathieu QW with a fixed potential width parameter

Table 1 Variation of electron subband energy differences and dipole moment matrix elements depending on the adjustable physical parameters of the Mathieu QW

η (nm)$^{-1}$	$\Delta E = E_2 - E_1$ (meV)	M_{12} (nm)	$f_{12} = \lvert M_{12}\rvert^2 \Delta E$(nm^2 *meV)
0.05	50.9345	2.70631	373.05
0.085	82.8373	2.21025	404.677
0.1	91.5812	2.13446	417.237
V_0 (meV)	$\Delta E = E_2 - E_1$(meV)	M_{12} (nm)	$f_{12} = \lvert M_{12}\rvert^2 \Delta E$ (nm^2 *meV)
80	78.771	2.2391	394.924
100	91.5812	2.13446	417.237
120	103.251	2.04819	433.146

and this case can be ascribed to the enhanced nonlinear optical properties of the semiconductor material. Figure 5a brings out the variation of RRICs with the photon energy for various potential width parameter values of Mathieu QW with a fixed barrier height in the absence of external perturbations. The difference between the subband energies increases, since the increase in the value of the potential width parameter, increases the confinement effect. Hence, a blueshift occurs as the structure parameter increases, that is, the peak position of RRICs moves towards the higher energies. Further, it is noticed that the peak value of the RRICs reduces when the potential width parameter enhances [51]. Figure 5b displays the variation of RRICs with the photon energy for various barrier heights of Mathieu QW with a fixed potential width parameter in the absence of external perturbations. It is found that the position of the peak value of the RRICs shifts towards the higher photon energies and the peak value decreases when the values of barrier height increase. This is because of the reduction of transition matrix elements and the enhancement of energy difference between the energy levels with the increase in barrier height and it is shown in Table 2. The negative values of RRICs are achieved

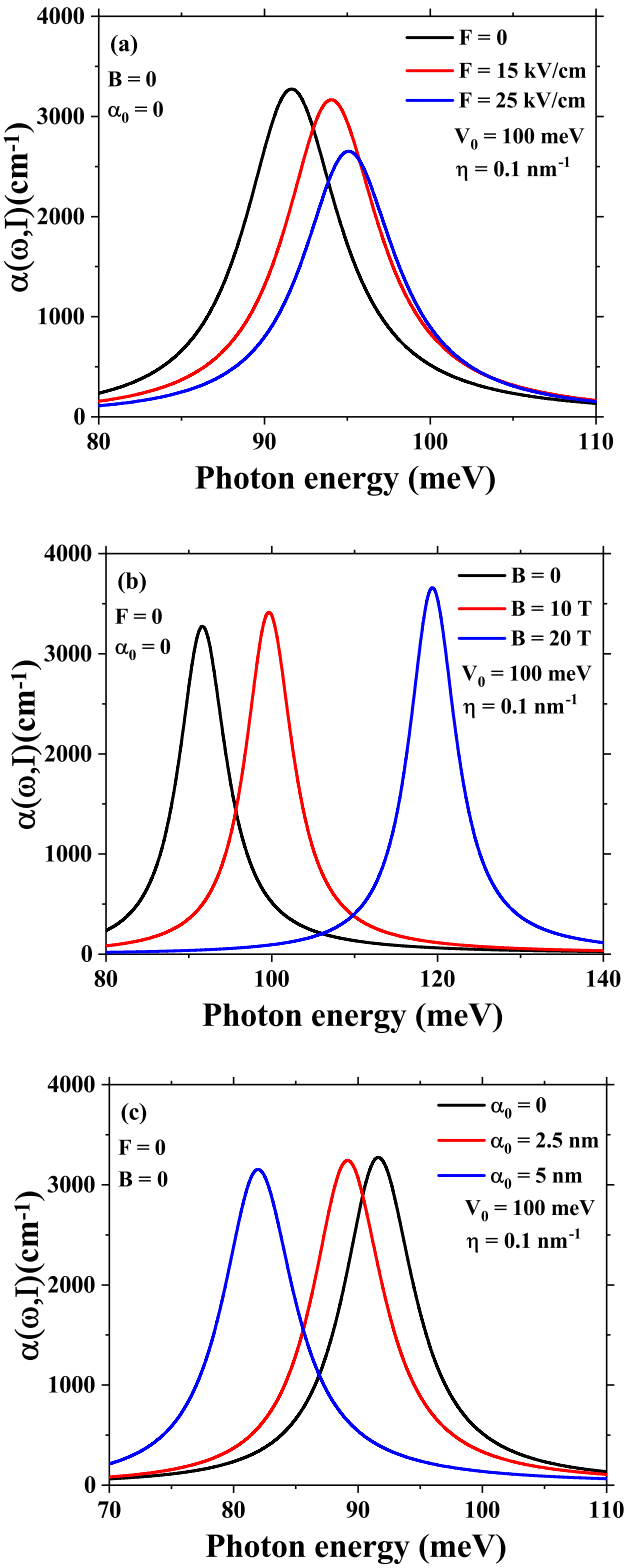

Fig. 4 Variation of TOACs with the photon energy for a constant potential width parameter and barrier height in Mathieu QW. Figure 4a shows the variation in the presence of an electric field without a magnetic field and ILF. Figure 4b shows the variation in the presence of a magnetic field without an electric field and ILF. Figure 4c shows the variation in the presence of ILF without a magnetic field and electric field

because the RRICs which are a combination of linear and nonlinear terms, decrease due to the negative contribution of the nonlinear term [52].

Figure 6 shows the changes of RRICs with the photon energy for a constant potential width parameter and barrier height in Mathieu QW. The change of RRICs as a function of photon energy in the presence of an electric field without a magnetic field and ILF are shown in Fig. 6a. It is observed that the peak of the RRICs moves towards the higher photon energies when the electric field

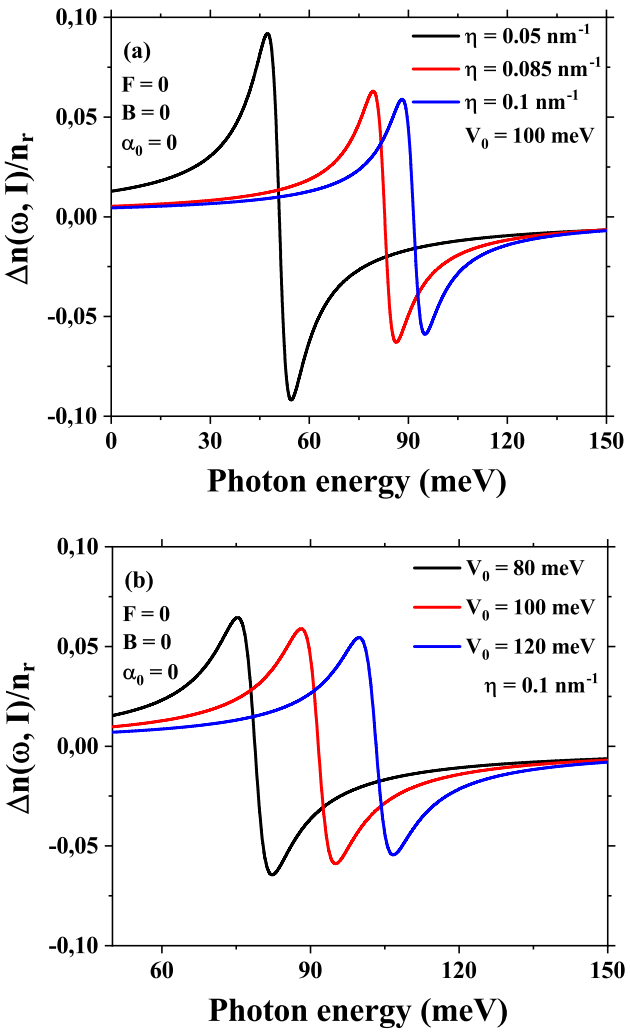

Fig. 5 Variation of RRICs with the photon energy in the absence of external perturbations. Figure 5a is for various potential width parameter values of Mathieu QW with a fixed barrier height. Figure 5b is for various barrier heights of Mathieu QW with a fixed potential width parameter

Table 2 Variation of electron subband energy differences and dipol moment matrix elements of the Mathieu QW according to externally applied static electric (F), magnetic (B), and THz intense laser field (α_0)

F(kV/cm)	$\Delta E = E_2 - E_1$(meV)	M_{12} (nm)	$f_{12} = \lvert M_{12}\rvert^2 \Delta E$(nm^2 *meV)
0	91.5812	2.13446	417.237
15	93.9732	2.06531	400.843
25	95.0229	1.8618	329.378
B(T)	$\Delta E = E_2 - E_1$(meV)	M_{12} (nm)	$f_{12} = \lvert M_{12}\rvert^2 \Delta E$(nm^2 *meV)
0	91.5812	2.13446	417.237
10	99.6033	2.08473	432.886
20	119.33	1.96059	458.694
α_0(nm)	$\Delta E = E_2 - E_1$(meV)	M_{12} (nm)	$f_{12} = \lvert M_{12}\rvert^2 \Delta E$(nm^2 *meV)
0	91.5812	2.13446	417.237
2.5	89.0997	2.15659	414.392
5	81.9033	2.22622	405.917

increases, that is, it forms a blueshift in the resonant peak. It is due to the enhancement of repulsion of effective potential with the increase in electric field and eventually, the potential becomes narrow on the left of the well. Thus, this new potential enlarges the distance between bound state energies which causes the movement to higher photon energies [53]. Figure 6b shows the change of RRICs as a function of photon energy in the presence of a magnetic field without an electric field and ILF. As can be seen from this figure and the values in Table 2, the increase in the magnetic field causes the peak position to shift to high energy due to the increase in the difference between the relevant energy levels, and the resonance peak to decrease due to the decrease in the transition matrix

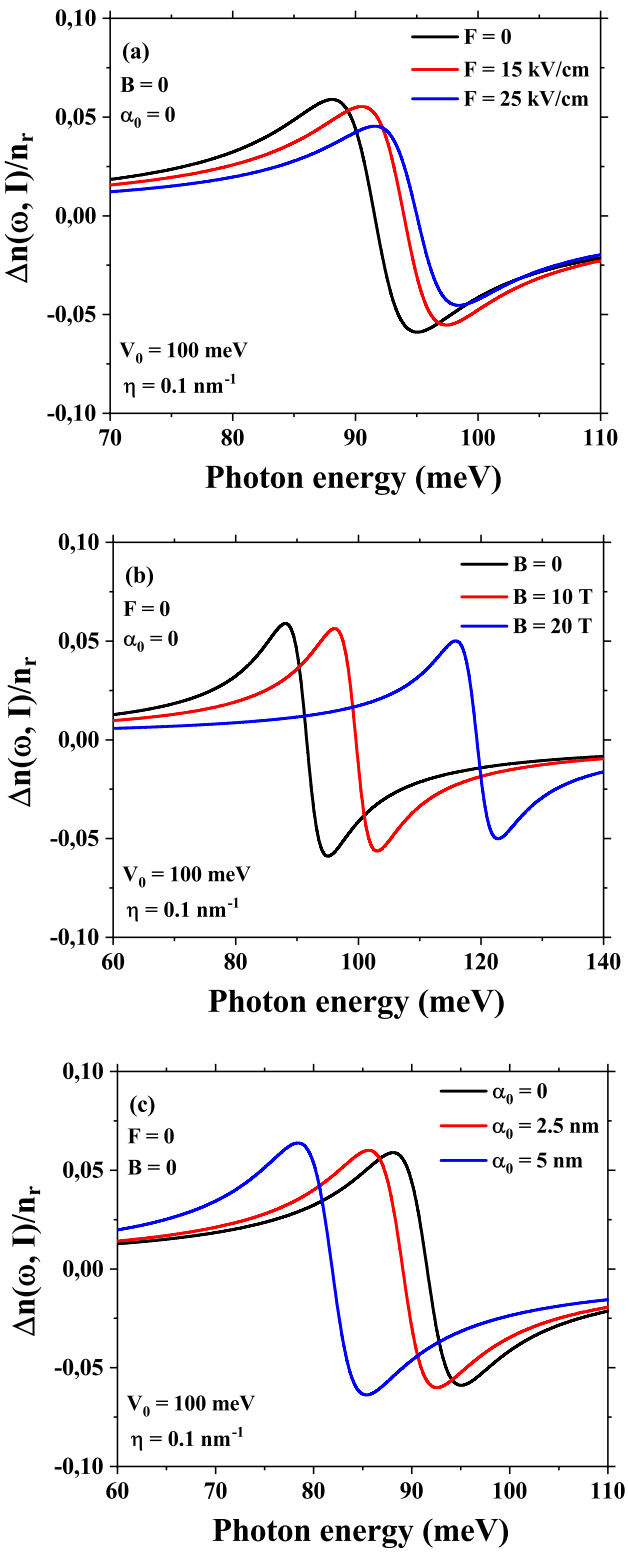

Fig. 6 Variation of RRICs with the photon energy for a constant potential width parameter and barrier height in Mathieu QW. Figure 6a shows the changes in the presence of an electric field without a magnetic field and ILF. Figure 6b shows the changes in the presence of a magnetic field without an electric field and ILF. Figure 6c shows the changes in the presence of ILF without a magnetic field and electric field

elements. Figure 6c shows the change of RRICs as a function of photon energy in the presence of ILF without magnetic field and electric field. It is noted that resonance peaks of the RRICs shifts towards the lower energies and their magnitude increases with the increase of laser field intensities. This is because the energy interval decreases, and the dipole matrix element increases with increasing the laser dressing parameter.

4 Conclusion

In conclusion, the effect of external perturbations such as electric, magnetic, and non-resonant THz intense laser fields on the total optical absorption coefficients and the relative refractive index changes of Mathieu potential quantum wells have been theoretically investigated. Further, the study on the influence of the adjustable physical parameters of the structure on the nonlinear optical properties of the system has also been carried out. The quantum well electronic subband energy levels and their envelope wave functions have been computed using the diagonalization method within the framework of the effective mass and parabolic single-band approximation. Then, expressions derived within the compact-density-matrix formalism have been employed to evaluate the optical properties of the Mathieu quantum well. The obtained numerical results show that the increase in both the structure parameters and the value of the electric and magnetic field shift the positions of the total optical absorption coefficients and relative refractive index changes towards higher energies (blue shift). On the other hand, the increase in the value of the intense laser field pushes the resonant peak positions to lower energy levels (red shift). The proposed theoretical model, with the structural parameters and employed approaches, can be applied to any arbitrary spatial constraints. The ranges of obtained parameters in the present study could pave the way to further experimental research works on the subject.

Data Availability Statement This manuscript has associated data in a data repository. [Authors' comment: The authors confirm that the data supporting the findings of this study are available within the article].

References

1. M.K. Gurnick, T.A. De Temple, IEEE J. Quant. Electron. QE. **19**, 791 (1983)
2. E.F. Schubert, J. Vac, Sci. Technol. A. **8**, 2980 (1990)
3. K. Ploog, M. Hauser, A. Fischer, Appl. Phys. A **45**, 233 (1988)
4. A.C. Maciel, M. Tatham, J.F. Ryan, J.M. Worlock, R.E. Nahory, J.P. Harbison, L.T. Forlez, Surf. Sci. **228**, 251 (1990)
5. L. Ioriatti, Phys. Rev. B **41**, 8340 (1990)
6. J.C. Egues, J.C. Barbosa, A.C. Notari, P. Basmaji, L. Ioriatti, E. Ranz, J. Portal, J. Appl. Phys. **70**, 3678 (1991)
7. M.H. Degani, Phys. Rev. B **44**, 5580 (1991)
8. M.H. Degani, J. Appl. Phys. **70**, 4362 (1991)
9. M.L. Ke, J.S. Rimmer, B. Hamilton, J.H. Evans, M. Missous, K.E. Singer, P. Zalm, Phys. Rev. B **45**, 14114 (1992)
10. M.L. Ke, J.S. Rimmer, B. Hamilton, M. Missous, B. Khamsehpour, J.H. Evans, K.E. Singer, P. Zalm, Surf. Sci. **267**, 65 (1992)
11. F. Vigneau, R. Mizokuchi, D. Zanuz, X. Huang, S. Tan, R. Maurand, S. Frolov, A. Sammak, G. Scappucci, F. Leoch, S. De Franceschi, Nano Lett. **19**, 1023 (2019)
12. C. Canedy, W. Bewley, C. Merritt, C. Kim, M. Kim, M. Warren, E. Jackson, J. Nolde, C. Aouda, E. Aifer, I. Vurgaftman, J. Meyer, Opt. Express. **27**, 3771 (2019)
13. U. Muhammad, M. Urooj, Z. Dong-Guang, H. Dong-Pyo, R. Muhammad, M. Nazeer, Appl. Sci. **9**, 1 (2019)
14. R.F. Kazarinov, R.A. Suris, Sov. Phys. Semicond. **5**, 707 (1971)
15. D.A.B. Miller, Int. J. High Speed Electron. **1**, 19 (1991)
16. S.Y. Yuen, Appl. Phys. Lett. **43**, 813 (1983)
17. F. Ungan, S. Pal, M.K. Bahar, M.E. Mora-Ramos, Superlattices Microstruct. **130**, 76 (2019)
18. I. Karabulut, H. Safak, M. Tomak, J. Appl. Phys. **103**, 103116 (2008)
19. I. Karabulut, U. Atav, H. Safak, M. Tomak, Eur. Phys. J. B **55**, 283 (2007)
20. I. Karabulut, H. Safak, Phys. B **368**, 82 (2005)
21. W.F. Xie, Phys. Stat. Sol. B **246**, 2257 (2009)
22. R.H. Wei, W.F. Xie, Curr. Appl. Phys. **10**, 757 (2010)
23. S. Baskoutas, E. Paspalakis, A.F. Terzis, J. Phys. Condens. Matter **19**, 395024 (2007)
24. S. Baskoutas, C. Garoufalis, A.F. Terzis, Eur. Phys. J. B **84**, 241 (2011)
25. S. Baskoutas, A.F. Terzis, Eur. Phys. J. B **69**, 237 (2009)
26. L. Lu, W. Xie, Z. Shu, Combined effects of hydrostatic pressure and temperature on nonlinear properties of an exciton in a spherical quantum dot under the applied electric field. Phys. B Condens. Matter **406**, 3735–3740 (2011)
27. E. Ozturk, I. Sokmen, Nonlinear intersubband absorption and refractive index changes in square and graded quantum well modulated by temperature and Hydrostatic pressure. J. Lumin. **134**, 42–48 (2013)
28. M. Kirak, Y. Altinok, S. Yilmaz, The effects of the hydrostatic pressure and temperature on binding energy and optical properties of a donor impurity in a spherical quantum dot under external electric field. J. Lumin. **136**, 415–421 (2013)
29. I. Karabulut, M.E. Mora-Ramos, C.A. Duque, Nonlinear optical rectification and optical absorption in GaAs–Ga1–xAlxAs asymmetric double quantum wells: combined effects of applied electric and magnetic fields and hydrostatic pressure. J. Lumin. **131**, 1502–1509 (2011)
30. J.C. Martínez-Orozco, M.E. Mora-Ramos, C.A. Duque, Nonlinear optical rectification and second and third harmonic generation in GaAs δ-FET systems under hydrostatic pressure. J. Lumin. **132**, 449–456 (2012)
31. G. Rezaei, S. Shojaeian Kish, Linear and nonlinear optical properties of a hydrogenic impurity confined in a two-dimensional quantum dot: effects of hydrostatic pressure, external electric and magnetic fields. Superlattices Microstruct. **53**, 99–112 (2013)
32. O. Aytekin, S. Turgut, M. Tomak, Nonlinear optical properties of a Pöschl-Teller quantum well under electric and magnetic fields. Phys. E **44**, 1612–1616 (2012)
33. L. Zhang, H.-J. Xie, Electric field effect on the second-order nonlinear optical properties of parabolic and semiparabolic quantum wells. Phys. Rev. B **68**, 235315 (2003)
34. A. Keshavarz, M.J. Karimi, Linear and nonlinear intersubband optical absorption in symmetric double semi-parabolic quantum wells. Phys. Lett. A **374**, 2675–2680 (2010)

35. A. Salman Durmuslar, A. Turkoglu, M.E. Mora-Ramos, F. Ungan, The non-resonant intense laser field effects on the binding energies and the nonlinear optical properties of a donor impurity in Rosen–Morse quantum well, Indian J. Phys. (2022)
36. İ Karabulut, S. Baskoutas, Linear and nonlinear optical absorption coefficients and refractive index changes in spherical quantum dots: effects of impurities, electric field, size, and optical intensity. J. Appl. Phys. **103**, 073512 (2008)
37. D. Altun, O. Ozturk, B.O. Alaydin, E. Ozturk, Linear and nonlinear optical properties of a superlattice with periodically increased well width under electric and magnetic fields. Micro Nanostruct. 207225 (2022)
38. H. Dakhlaoui, M. Nefzi, Superlattices Microstruct. **136**, 106292 (2019)
39. U. Yesilgul, E.B. Al, J.C. Martínez-Orozco, R.L. Restrepo, M.E. Mora-Ramos, C.A. Duque, F. Ungan, E. Kasapoglu, Linear and nonlinear optical properties in an asymmetric double quantum well under intense laser field: effects of applied electric and magnetic fields. Opt. Mater. **58**, 107–112 (2016)
40. F. Ungan, M.E. Mora-Ramos, E. Kasapogluc, H. Sari, I. Sökmen, Nonlinear optical properties of triple δ-doped quantum wells: the impact of the applied external fields. Optik **180**, 387–393 (2019)
41. P. Başer, M.K. Bahar, Evaluation of the external electric- and magnetic field-driven Mathieu quantum dot's optical observables. Phys. B **639**, 413991 (2022)
42. J.-B. Xia, W.-J. Fan, Electronic structures of superlattices under in-plane magnetic field. Phys. Rev. B **40**, 8508–8515 (1989)
43. E.B. Al, F. Ungan, U. Yesilgul, E. Kasapoglu, H. Sari, I. Sökmen, Infrared transitions between hydrogenic states in GaInNAs/GaAs quantum wells. Int. J. Mod. Phys. B **30**, 1650139 (2016)
44. E.M. Goldys, J.J. Shi, Linear and nonlinear intersubband optical absorption in a strained double barrier quantum well. Phys. Status Solidi B **210**, 237–248 (1998)
45. D. Ahn, S.L. Chuang, Calculation of linear and nonlinear intersubband optical absorptions in a quantum well model with an applied electric field. IEEE J Quantum Electron QE **23**, 2196–2204 (1987)
46. S. Unlu, I. Karabulut, H. Safak, Linear and nonlinear intersubband optical absorption coefficients and refractive index changes in a quantum box with finite confining potential. Phys. E **33**, 319–324 (2006)
47. H. Sari, E.B. Al, E. Kasapoglu, S. Sakiroglu, I. Sökmen, M. Toro-Escobar, C.A. Duque, Electronic and optical properties of a D^{2+} complex in two-dimensional quantum dots with Gaussian confinement potential. Eur. Phys. J. Plus **137**, 464 (2022)
48. E.B. Al, E. Kasapoglu, H. Sari, I. Sökmen, Optical properties of spherical quantum dot in the presence of donor impurity under the magnetic field. Phys. B **613**, 412874 (2021)
49. P. Hashemi, M. Servatkhah, R. Pourmand, The effect of Rashba spin-orbit interaction on optical far-infrared transition of tuned quantum dot/ring systems. Opt. Quant. Electron. **53**, 567 (2021)
50. A.N. Aishah, H. Dakhlaoui, T. Ghrib, B.M. Wong, Phys. B **635**, 413838 (2022)
51. M.K. Bahar, P. Başer, Micro Nanostruct. **170**, 207371 (2022)
52. L. Máthé, C.P. Onyenegecha, A.A. Farcaş, L.M. Pioraş-Ţimbolmaş, M. Solaimani, H. Hassanabadi, Phys. Lett. A **397**, 127262 (2021)
53. P. Başer, M.K. Bahar, Phys. B **639**, 413991 (2022)